# Fusion of EEG and fMRI via Soft Coupled Tensor Decompositions

Christos Chatzichristos[1,2], Mike Davies[3], Javier Escudero[3], Eleftherios Kofidis[4,2], Sergios Theodoridis[1,2]
[1]Dept. of Informatics and Telecommunications, University of Athens, Greece (stheodor@di.uoa.gr)
[2]Computer Technology Institute & Press "Diophantus" (CTI), Greece (chatzichris@cti.gr)
[3] Inst. of Digital Communications, School of Engineering, University of Edinburgh, UK ({mike.davies,javier.escudero}@ed.ac.uk)
[4] Dept. of Statistics and Insurance Science, University of Piraeus, Greece (kofidis@unipi.gr)

***Abstract*—Data fusion refers to the joint analysis of multiple datasets which provide complementary views of the same task. In this paper, the problem of jointly analyzing electroencephalography (EEG) and functional Magnetic Resonance Imaging (fMRI) data is considered. Analyzing both EEG and fMRI measurements is highly beneficial for studying brain function because these modalities have complementary spatiotemporal resolutions: EEG offers good temporal resolution while fMRI offers good spatial resolution. The fusion methods reported so far ignore the underlying multi-way nature of the data in at least one of the modalities and/or rely on very strong assumptions concerning the relation among the respective data sets. In this paper, these two points are addressed by adopting tensor models for both modalities and by following a soft coupling approach to implement the fused analysis. To cope with the subject variability in EEG, the PARAFAC2 model is adopted. The results obtained are compared against those of Parallel ICA and hard coupling alternatives in both simulated and real data. Our results confirm the superiority of tensorial methods over methods based on ICA. In scenarios that do not meet the assumptions underlying hard coupling, the advantage of soft coupled decompositions is clearly demonstrated.**

## I. Introduction

In an attempt to better understand a system as complex as the human brain, multimodal measurements can be beneficial since they are able to provide information on complementary aspects of the same system. Through jointly analyzing the data from different modalities, their individual advantages may be exploited and at the same time some of their disadvantages are mitigated [1, 2]. In this way, a more accurate localization of the activated brain areas can be obtained. This turns out to be a challenging Blind Source Separation (BSS) problem [3, 4].

Two of the most commonly used modalities for monitoring the brain activity are the electroencephalography (EEG) and the functional Magnetic Resonance Imaging (fMRI). fMRI is a noninvasive brain imaging technique, which indirectly studies brain activity by measuring fluctuations of the blood-oxygen-level dependent (BOLD) signal [5]. BOLD fluctuation usually occurs between 3 to 10 seconds after the stimulus, and this effect is modeled by the so-called haemodynamic response function (HRF). Although fMRI has a high spatial resolution, often at the millimeter scale, it is a "delayed" measure of the brain activity, with its temporal resolution being limited by the repetition time of the scanner (TR), usually of the order of seconds [5]. The EEG signal results from the electrical measurement of neural activities realized through the movement of charged ions at the junction between the synapses of neurons. This provides a more direct measure of the neuronal activity compared to fMRI, sensitive to millisecond changes in neural processing, and hence a better temporal resolution. However, EEG has poor spatial resolution, limited by the number of electrodes employed and the resistive properties of the extracerebral tissues. Furthermore, due to the fact that electrodes are more sensitive to neural activations that occur closer to the scalp, the determination of the exact location of activations that take place in deeper areas is more challenging [6]. The complementary nature of their spatiotemporal resolutions motivates the fusion of EEG and fMRI on the way to a better localization of the brain activity, both in time and space [4, 7].

Different types of fusion can be realized [1, 7, 8]. The earliest approaches for fusion of fMRI and EEG (and a large number of recent ones, e.g., [9]) are essentially "integrative" in nature. The rationale behind these methods is to employ objective functions for decomposition of the fMRI signal with constraints based on information from EEG (or vice versa). Recently, the emphasis has been turned to "true" fusion, e.g., [7, 10, 11, 12, 13, 14], where the decomposition of the data from each modality can influence the other using all the common information that may exist. During optimization the factors, which have been identified as shared, are appropriately "coupled" and thus a bridge between the two modalities is established. Various ways to realize the coupling have been proposed depending on the coupled mode: a) coupling at the spatial domain with the use of the so-called lead-field matrix, which summarizes the volume conduction effects in the head [7], b) coupling at the time domain using the convolution with an HRF [13, 14], and c) coupling at the subjects domain, using the assumption that the same neural processes are reflected in both modalities with the same covariation [10, 15, 16]. In all the aforementioned methods, the coupling between the corresponding modes is "hard", meaning that the shared factors are equal in the two datasets.

Multivariate bi-linear (i.e., matrix-based) methods, mainly based on Independent Component Analysis (ICA) [16, 17, 18, 19] and relying on the concatenation of different modes, have been, up to recently, the state of the art for jointly analyzing EEG and fMRI. However, by definition such methods fall short in exploiting the multi-way nature of the data. fMRI and EEG datasets are inherently multi-dimensional, comprising information in time and along different voxels or channels, subjects, trials, etc. For EEG, in order to better exploit the information, the signal can be expanded in additional dimensions, e.g. through incorporating spectral features by computing a wavelet transform of the EEG data or using the segment/Event Related Potential (ERP) mode (ERP is the response to a specific sensory, cognitive, or motor stimulus) [20]. This multi-dimensional nature of the EEG and fMRI datasets points to the adoption of tensor (multi-linear) models instead of the bi-linear ones. Several tensor decomposition methods have been applied in fMRI and EEG BSS, including Canonical Polyadic Decomposition (CPD) or Parallel Factor Analysis (PARAFAC) [21, 22] and its generalization known as PARAFAC2 [23, 24]. The unique representations that are possible with tensor models can improve the ability of extracting spatiotemporal modes of interest and facilitate subsequent interpretations that are neurophysiologically meaningful [25]. Furthermore, CPD and PARAFAC2 are deterministic, hence free of statistical assumptions and able to work with smaller data sizes than statistical methods. Moreover, they are able to make predictions more robustly in the presence of noise, compared to their two-way counterparts [21, 26]. Note that the biomedical data are usually highly corrupted by noise [21].

ISBN 978-90-827970-1-5 

Although the multi-way nature of EEG has been exploited in earlier fusion methods [10, 11], it has been neglected for fMRI. Furthermore, these methods rely on preprocessing of the fMRI data using the General Linear Model (GLM) framework. A spatial map of interest (areas of activation) per subject is extracted from the fMRI data and all the spatial maps are stacked into a matrix (space $\times$ subjects), hence discarding the extra dimension of time and relying on Coupled Matrix Tensor Factorization (CMTF) to solve the joint BSS problem.[1] In the GLM framework, a canonical HRF was assumed to be known (and invariant in space and among subjects), the expected signal changes are defined as regressors of interest in a multiple linear regression analysis and the estimated coefficients are tested against a null hypothesis. Intra- and inter-subject variability of HRF is known to exist [27], hence a possible misspecification of the HRF may lead to biased estimates of widespread activity in the brain [5, 27]. Moreover, the mismatch of the temporal characteristics of EEG and fMRI further limits the potential of GLM analysis [19]. The use of the spatial maps of GLM categorizes such CMTF-based methods as "late" fusion [8] or true fusion using multivariate features [1].

In this paper, we propose true "early" [8] fusion of fMRI and EEG tensors via soft (assuming similarity and not strong-hard equality) coupling among modes. In our approach, we exploit the multi-way nature of both modalities and omit the GLM preprocessing step, in an effort to fully exploit the information underlying the raw data [1, 8]. We demonstrate, with simulated data, the advantage of the proposed method over methods based on Independent Component Analysis (ICA), hard coupling and uncoupled CPD per modality. In the last part, the proposed method is tested in an oddball paradigm with real data and the results obtained are compared with those of the traditional analysis of the ERPs.

### A. Notation

Vectors, matrices and higher-order tensors are denoted by bold lower-case, upper-case and calligraphic upper-case letters, respectively. For a matrix $\mathbf{A}$, $\mathbf{A}^\top$ denotes its transpose. The symbol $\odot$ denotes the Khatri-Rao product of two matrices, $\boldsymbol{A} \in \boldsymbol{R}^{I\times R}$ and $\boldsymbol{B} \in \boldsymbol{R}^{J\times R}$, namely $\boldsymbol{A} \odot \boldsymbol{B} = [\boldsymbol{a}_1 \otimes \boldsymbol{b}_1, \boldsymbol{a}_2 \otimes \boldsymbol{b}_2, \ldots, \boldsymbol{a}_R \otimes \boldsymbol{b}_R]$, with $\boldsymbol{a}_i, \boldsymbol{b}_i$ being the $i$th columns of $\boldsymbol{A}, \boldsymbol{B}$, respectively, and $\otimes$ denoting the Kronecker product. The outer product is denoted by $\circ$.

## II. Methods

### A. Canonical Polyadic Decomposition (CPD)

CPD (or PARAFAC) [26] approximates a 3rd-order tensor, $\boldsymbol{\mathcal{T}} \in \mathbb{R}^{I_1\times I_2\times I_3}$ (naturally extended to tensors of higher order), by a sum of $R$ rank-1 tensors,

$$\boldsymbol{\mathcal{T}} \approx \sum_{r=1}^{R} \boldsymbol{a}_r \circ \boldsymbol{b}_r \circ \boldsymbol{c}_r \tag{1}$$

Equivalently, for the $k$th frontal slice of $\boldsymbol{\mathcal{T}}$,

$$\boldsymbol{T}_k \approx \boldsymbol{A}\boldsymbol{D}_k\boldsymbol{B}^\top, \quad k = 1, 2, \ldots, I_3 \tag{2}$$

where $\boldsymbol{A} = [\boldsymbol{a}_1, \boldsymbol{a}_2, \ldots, \boldsymbol{a}_R]$, $\boldsymbol{B}$ and $\boldsymbol{C}$ are similarly defined matrices, and $\boldsymbol{D}_k$ is the diagonal matrix having the elements of the $k$th row of $\boldsymbol{C}$ on its diagonal. The main advantage of the CPD, besides its simplicity, is the fact that it is unique (up to permutation and scaling) under mild conditions [26]. Uniqueness of CPD is crucial to its application in BSS problems. Its performance is, however, largely dependent on the correct estimation of the tensor rank, $R$, and for its determination several heuristic methods have been proposed [28].

[1] Advanced CMTF (ACMTF) [11, 12] allows the presence of both shared and unshared components in the coupled factor(s) and provides a way to automatically determine them.

### B. PARAFAC2

PARAFAC2 [26] differs from CPD in that strict multilinearity is no longer a requirement. CPD applies the same factors across all the different modes, whereas PARAFAC2 relaxes this constraint and allows variation across one of the modes (in terms of the values and/or the size of the corresponding factor matrix). For this reason, PARAFAC2 is not a tensor model in the strict sense as it can represent both regular tensors, with weaker constraints than CPD, as well as irregular tensors (collections of matrices of different dimensions) with size variations along one of the modes. It can be written in terms of the (here frontal) slices of the tensor $\boldsymbol{\mathcal{T}}$ as

$$\boldsymbol{T}_k \approx \boldsymbol{A}_k\boldsymbol{D}_k\boldsymbol{B}^\top, \quad k = 1, 2, \ldots, I_3, \tag{3}$$

with $\boldsymbol{A}_k$ being different for different $k$'s. This type of decomposition is clearly non-unique. Thus, in order to allow for uniqueness, it has been proposed to add the constraint that the cross products $\boldsymbol{A}_k^\top\boldsymbol{A}_k$ be constant over $k$. This has been shown [29] to be equivalent to setting $\boldsymbol{A}_k = \boldsymbol{P}_k\boldsymbol{H}$, where the $R\times R$ matrix $\boldsymbol{H}$ is the same for all slices, while the variability is represented by the columnwise orthonormal $I_2 \times R$ matrix $\boldsymbol{P}_k$. Under this constraint, one has to fit the equivalent model

$$\boldsymbol{P}_k^\top\boldsymbol{T}_k \approx \boldsymbol{H}\boldsymbol{D}_k\boldsymbol{B}^\top, \quad k = 1, 2, \ldots, I_3. \tag{4}$$

As shown in [29], $\boldsymbol{P}_k$ can be computed as $\boldsymbol{P}_k = \boldsymbol{V}_k\boldsymbol{U}_k^\top$, where $\boldsymbol{U}_k$ and $\boldsymbol{V}_k$ are the left and right singular matrices of $\boldsymbol{H}\boldsymbol{D}_k\boldsymbol{B}^\top\boldsymbol{T}_k^\top$. As can be seen from Eq. (4), the problem of fitting PARAFAC2 has been transformed into that of fitting a CPD model with transformed data. Applications of PARAFAC2 in fMRI and EEG analysis include [9, 23] and [24], respectively.

### C. ICA-based methods

Classical approaches for jointly analyzing fMRI and EEG include Joint Independent Component Analysis (JICA) (using one [15, 17] or multiple [16] electrodes for EEG), and Parallel ICA [17, 19]. JICA jointly analyzes data from the same subjects from both modalities simultaneously. To achieve this, it uses the features derived from the first-level analysis of fMRI (spatial maps) and the averaged ERP epochs of EEG, hence JICA is also classified as a late true fusion model. JICA assumes that a stronger ERP yields a stronger BOLD fluctuation in the same area (and vice versa), which supports the common assumption of having the same linear mixing system in the two modalities (in the subjects domain). Furthermore, each pair of shared components is assumed to be dependent between the modalities and at the same time statistically independent of the rest of the components [18]. Parallel ICA first identifies components separately for each modality, performing a temporal ICA in EEG and a spatial ICA in fMRI. At a second step, the corresponding extracted components are identified based on their correlation in the temporal domain. Parallel ICA can be computed either at a single-subject level [19] or at a multi-subject level using Group ICA [30].

## III. Soft Coupled Tensor Decompositions

Coupling through equality (hard coupling), which is used both in CMTF-based methods [10, 11, 12] and in JICA [15, 16, 18] approaches, arises from the assumption that the neural sources are reflected (with the same power) in both modalities; however this is restrictive. Even if the exact equality and the independence assumptions, used by JICA, are valid, still the result of the first-level analysis of fMRI (used as an initial

ISBN 978-90-827970-1-5 © EURASIP 2018

step [10, 11, 12, 15, 16, 18]) is not taking into account the complementary information of EEG. Furthermore, as reported in [18], the result obtained with JICA is mostly influenced by the quality of the ERPs (EEG) and less by the fMRI data. This may indicate that information, which could not be retrieved by GLM, is "hidden" in the raw fMRI data and not in the spatial maps, which inherit the drawbacks of GLM [5].

We propose a framework for early fusion of fMRI and EEG using coupled CPD with "soft" coupling [31], which means similarity and not exact equality. Fusion based on raw data, although potentially quite challenging, may allow better inference [8]. The coupling could be attempted in any of the modes, depending on the problem at hand.

The CPDs of the 3rd-order fMRI tensor, $\boldsymbol{\mathcal{T}} \in \mathbb{R}^{I_a \times I_b \times I_3}$, and the 4th-order EEG tensor, $\tilde{\boldsymbol{\mathcal{T}}} \in \mathbb{R}^{I_e \times I_1 \times I_2 \times I_3}$, can be written as $\boldsymbol{T}_k \approx \boldsymbol{A}\boldsymbol{D}_k\boldsymbol{B}^\top$ and $\tilde{\boldsymbol{T}}_{k(1)} \approx \boldsymbol{E}\tilde{\boldsymbol{D}}_k(\tilde{\boldsymbol{B}} \odot \tilde{\boldsymbol{A}})^\top$, respectively, with $\tilde{\boldsymbol{T}}_{k(1)}$ being the mode-1 matricization of $\tilde{\boldsymbol{\mathcal{T}}}_k = \tilde{\boldsymbol{\mathcal{T}}}(:,:,:,k)$ [23]. $\boldsymbol{A} = [\boldsymbol{a}_1, \boldsymbol{a}_2, \ldots, \boldsymbol{a}_R]$ is a matrix that contains the weights of the $R$ spatial components ($I_a$ voxels), $\boldsymbol{B}, \boldsymbol{C}$ contain the associated time courses ($I_b$) and subject activation levels of fMRI ($I_3$), respectively, and $\boldsymbol{D}_k$ is the diagonal matrix formed from the $k$th row of $\boldsymbol{C}$. For the EEG case, matrices $\boldsymbol{E}, \tilde{\boldsymbol{A}}, \tilde{\boldsymbol{B}}, \tilde{\boldsymbol{C}}$ contain the weights of the associated ERPs ($I_e$), electrodes ($I_1$), trials amplitude ($I_2$) and the subject activation levels of EEG ($I_3$), respectively, and $\tilde{\boldsymbol{D}}_k$ is the diagonal matrix formed from the $k$th row of $\tilde{\boldsymbol{C}}$. The proposed cost function to minimize is given as

$$\begin{aligned}&\sum_{k=1}^{I_3} \|\boldsymbol{T}_k - \boldsymbol{A}\boldsymbol{D}_k\boldsymbol{B}^\top\|_F^2 + \sum_{k=1}^{I_3} \|\tilde{\boldsymbol{T}}_{k(1)} - \boldsymbol{E}\tilde{\boldsymbol{D}}_k(\tilde{\boldsymbol{B}} \odot \tilde{\boldsymbol{A}})^\top\|_F^2 \\ &+ \lambda_A \|\boldsymbol{L}\boldsymbol{A}_{1:R_c} - \tilde{\boldsymbol{A}}_{1:R_c}\|_F^2 + \lambda_B \|\boldsymbol{B}_{1:R_c} - \boldsymbol{H}\tilde{\boldsymbol{B}}_{1:R_c}\|_F^2 \\ &+ \lambda_C \|\boldsymbol{C}_{1:R_c} - \tilde{\boldsymbol{C}}_{1:R_c}\|_F^2,\end{aligned} \tag{5}$$

with $\boldsymbol{L}$ being the lead-field matrix used for the EEG forward problem and $\boldsymbol{H}$ the matrix representing the convolution with the HRF and the down-sampling (due to the different sampling rate of the two modalities). $R_c$ is the number of common components in the coupled mode(s), so there are $R - R_c$ and $\tilde{R} - R_c$ distinct components of fMRI and EEG, respectively. In this way, different model orders can be assigned to the decompositions of the modalities as long as the number of common components remains the same (without loss of generality, in (5), we assume that the common components are the first $R_c$ ones). In order to estimate $R_c$, $\boldsymbol{\mathcal{T}}$ and $\tilde{\boldsymbol{\mathcal{T}}}$ are separately decomposed, and a correlation matrix is computed based on the coupled modes of the tensors. Components with similarity exceeding a predefined threshold $t$ comprise the common components [32]. From the same metric, we can get an indication for the appropriate $\lambda$ values(which quantify the degree of coupling) to be used: higher correlation indicates higher values for $\lambda$; hence the $\lambda$'s of the modes which will not be coupled will be set to zero. The data of both modalities must be normalized (to unit norm) beforehand (so that the first two terms in (5) have the same weight in the cost function) and preprocessed for removal of artifacts. For the initialization of the coupled tensors decomposition, the Generalized EigenValue Decomposition (GEVD)-based method proposed in [33] is used.[2] When prior information is available for any of the modes (or part of them), the respective columns can be excluded from the optimization function and set equal (or almost equal) to the known factors (see Section V).

As can be noted in Eq. (5), the quadrilinear model of CPD selected for decomposing the EEG tensor assumes that every subject has exactly the same ERP, an assumption which is restrictive [34] and can be overcome with the adoption of PARAFAC2 [34, 35], where $\boldsymbol{E}$ may vary with $k$. Thus, the CPD used for EEG can be replaced by PARAFAC2, with $\boldsymbol{E}_k = \boldsymbol{P}_k\boldsymbol{H}$ and $\boldsymbol{P}_k$ and $\boldsymbol{H}$ computed as in Section II.B, and the cost function (5) is transformed to:

$$\begin{aligned}&\sum_{k=1}^{I_3} \|\boldsymbol{T}_k - \boldsymbol{A}\boldsymbol{D}_k\boldsymbol{B}^\top\|_F^2 + \sum_{k=1}^{I_3} \|\boldsymbol{P}_k^\top\tilde{\boldsymbol{T}}_{k(1)} - \boldsymbol{H}\tilde{\boldsymbol{D}}_k(\tilde{\boldsymbol{B}} \odot \tilde{\boldsymbol{A}})^\top\|_F^2 \\ &+ \lambda_A \|\boldsymbol{L}\boldsymbol{A}_{1:R_c} - \tilde{\boldsymbol{A}}_{1:R_c}\|_F^2 + \lambda_B \|\boldsymbol{B}_{1:R_c} - \boldsymbol{H}\tilde{\boldsymbol{B}}_{1:R_c}\|_F^2 \\ &+ \lambda_C \|\boldsymbol{C}_{1:R_c} - \tilde{\boldsymbol{C}}_{1:R_c}\|_F^2.\end{aligned} \tag{6}$$

## IV. Simulated Data

A simulated dataset similar to the one used in [30] and [36] has been employed for our analysis. A disc with 2452 voxels (dipoles) was created in order to generate the data. For EEG, a concentric three-sphere model with 128 electrodes was set to wrap the disc, and the lead-field matrix computed in [36] has been used. The temporal sampling of EEG was 1 kHz while the epoch of the ERPs was set to 400 ms. The fMRI spatial maps were simulated as 2D images of $70 \times 70$ voxels, via the SimTB [37] toolbox and a Z-axis of 18 mm was adopted. In comparison to [30, 36], the overlap in time for EEG and in space for fMRI has been increased. In Fig. 1, the assumed neurophysiological sources can be viewed, from left to right: "vision area" S1, "default mode network" S2, "auditory cortex" S3, "sensory networks" S4, "cognition areas" S5 and "dorsal attention network" S6. These assumed active neural sources (rows a, b) along with the assumed ERPs (row d) yield scalp distributions and single-trial images in EEG and spatial maps and time-courses of fMRI. Single-trial images (row c) are generated by multiplying each ERP (row d) with the trial amplitude (row a). Scalp potential distribution maps (topoplots, row e) are computed by solving the forward problem for each spatial map of row a. The fMRI BOLD signals (time-courses, row f) were computed through the convolution between the trial amplitude (row a) with the canonical HRF. The results of different methods will be examined: Parallel ICA, uncoupled CPDs (separately decomposing each tensor), hard and soft coupling in the time domain with different $\lambda_B$ values (since only the time domain will be tested, $\lambda_A = \lambda_C = 0$). The computation of the proposed soft coupled decomposition was performed within the Structured Data Fusion (SDF) framework [38] of Tensorlab [39] and Parallel ICA was implemented (using Group ICA) as in [19, 30], based on InfoMax [40] for performing ICA.

In Fig. 2, the mean correlation between the obtained sources and the ground truth per method and per modality (diamonds

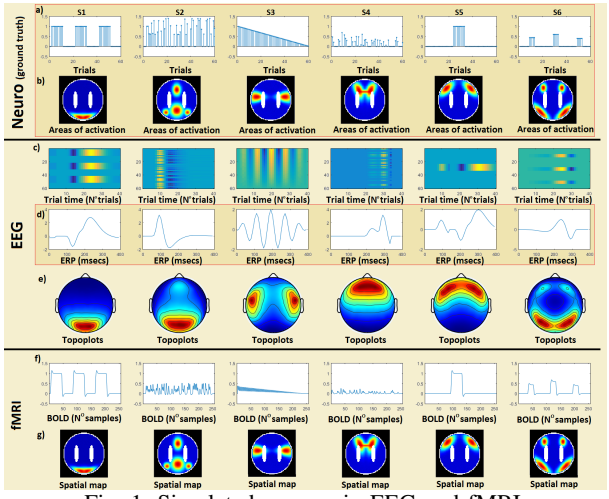


Fig. 1: Simulated sources in EEG and fMRI.

[2]Special thanks to Nico Vervliet, KU Leuven, for sharing the code by M. Sørensen, KU Leuven.

ISBN 978-90-827970-1-5 © EURASIP 2018

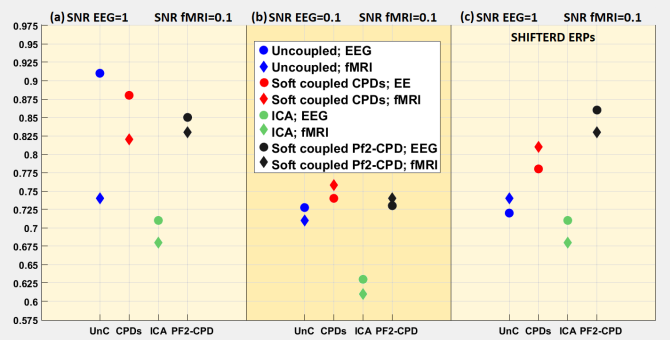


Fig. 2: Accuracy of different methods. EEG: diamonds, fMRI: discs for EEG and disks for fMRI) at different Signal to Noise Ratios (SNR= square of the amplitude ratio) can be observed. In cases (a) (same noise level as in [30]) and (b), different levels of noise are tested, while in case (c) the assumption of the same ERP per subject is invalidated and the ERPs are shifted. Parallel ICA exhibits inferior performance compared to both the uncoupled (Unc) and soft coupling methods (Coupled CPDs, "CPDs" and Coupled PARAFAC2 CPD, "PF2-CPD") in all of the cases, due to the overlapping in the sources, which invalidates the independence assumption. The resulting spatial maps obtained by spatial ICA in case (a) can be viewed in Fig. 3. Note that, in the areas of overlapping, there is crosstalk between the maps. S5, which overlaps with most of the rest of the sources, can not be identified (for comparison with the ground truth, observe row g of Fig. 1). It can be seen that, in case (a), the correlation for EEG with uncoupled analysis is higher than with soft coupling. This is caused by the performance gain for the fMRI source in the coupled case which results in a slight loss for EEG. Overall, the correlation is increased with soft coupling. In case (b), where the SNR is the same for both modalities, soft coupling yields better results. PF2-CPD in both (a) and (b) cases yields a slightly worse result than coupled CPDs (since the multilinearity assumption used by CPD is valid here). The last case, (c), is the one where the advantage of PARAFAC2 becomes apparent. We observe that ICA is affected from the ERP shifting much less than the uncoupled and the coupled CPD methods, but it still has the worst performance.

Fig. 4 visualizes the importance of the choice of the $\lambda_B$ value for soft coupling. We can note two cases. In the first case (the solid lines), where the coupling assumption is exact, it can be readily seen that the hard coupling is the best to use. However, the soft coupling analysis can reach the same performance with the appropriate tuning of $\lambda_B$. In this case, the simulated fMRI time-courses were generated via the convolution of trials with the canonical HRF. In the second case (dotted lines), the assumption of exact coupling is violated as the time-courses were generated by convolution with different HRFs (the 5 HRFs presented in [41] have been used), while $\boldsymbol{H}$ (Eq. (6)) was constructed based on the canonical HRF. The fact that the time courses are similar but not equal deteriorates the performance of the hard coupling. Hard coupling still performs better than the uncoupled version but it is outperformed by the soft coupling for $\lambda_B > 0.1$.

## V. Real Data

In this section, some preliminary results from the analysis of real data will be briefly reported. The dataset was obtained

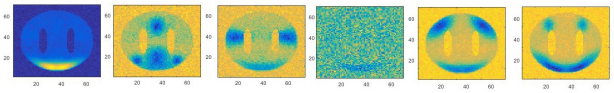

Fig. 3: Resulting fMRI spatial maps with ICA, at SNR=0.1.

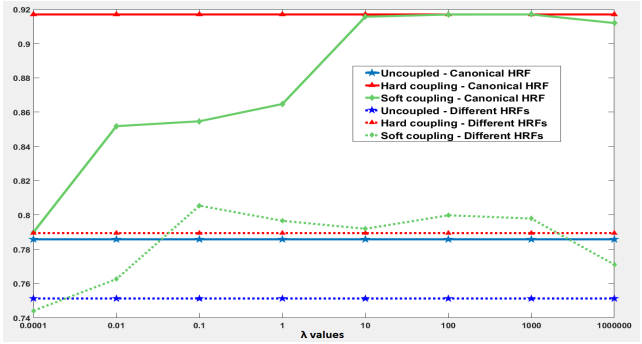


Fig. 4: Correlation of the obtained sources with Uncoupled, Hard coupled and Soft coupled CPDs with different $\lambda_B$ values.

from the OpenfMRI [42] database. Its accession number is ds000116 and it has been previously used in [43]. The 17 subjects performed separate, yet analogous in their design, auditory and visual oddball tasks (interleaved), while EEG-fMRI were simultaneously recorded. Despite the fact that the data was preprocessed and the authors mention that the ballistocardiac artifact has been removed, the data is still contaminated with leftovers. Thus, instead of attempting a pure BSS, we use the prior information, assuming that two of the components of the trial mode of the EEG are known and equal to the timings of the normal and oddball stimuli; hence, this corresponds to a semi-blind (guided) decomposition. We extracted 600 ms stimulus-locked epochs of the auditory task. For every subject, a sequence of 100 such epochs of interleaved normal and target (oddball) stimuli is formed, hence "creating" the same sequence for every subject in order to use the soft coupled CPD. The well known P300 [34] was the obtained ERP component of the rank-one tensor which includes the (known) time-course of the oddball stimuli. The P300 obtained exhibits higher amplitude than the one acquired from the traditional mean ERP analysis, with a peak at 420 ms (after the stimulus). The fMRI activations were mainly located at middle frontal gyrus, middle temporal gyrus, insula, parietal lobule, and anterior cingulate cortex, which are areas consistent with previous oddball research [43, 44]. The mean ERP analysis pointed out significant differences of the P300 among the different subjects and hence the application of the coupled PF2-CPD has been also evaluated. Higher activations in the left frontal gyrus and temporal gyrus resulted from the use of the non-multilinear model. However, the presence of high frequency noise in the components needs to be further examined. A more detailed account of this and other analyses with real data will be reported in a future publication. Figures with some preliminary results can be viewed at pix.sfly.com/MXKzXsMp.

## VI. Conclusions

In this paper, two different soft coupled tensor decomposition methods were investigated for jointly analyzing fMRI and EEG data. This is an attempt to benefit from the multi-way nature of *both* modalities, following an "early true" fusion (hence bypassing the need to rely on features). Performance gains have been reported compared to ICA methods as well as to the separate analyses of the datasets. The use of coupled PARAFAC2-CPD was seen to outperform the coupled CPD in the presence of shifts in the ERPs per subject. A simple mean-ERP analysis prior to the joint analysis could provide an indication of the amount of the shift in the ERPs, in order to select which of the soft coupled tensor decompositions shall be used. Future work will include more studies with real data, comparisons with methods based on Independent Vector Analysis (IVA) [2] and alternative tensor models (e.g., Block Term

ISBN 978-90-827970-1-5 © EURASIP 2018

Decomposition [45]). Moreover, a more systematic selection of the $\lambda$ values will be sought for.

## ACKNOWLEDGMENT

The authors would like to thank Dr. Li Dong, UEST, China for providing the lead-field matrix used in [36] and Dr. Loukianos Spyrou, Univ. of Edinburgh, UK and Nico Vervliet, KU Leuven, Belgium for fruitful discussions on the topics of EEG and soft coupling in Tensorlab, respectively. The research leading to these results was funded by the European Union's H2020 Framework Programme (H2020-MSCA-ITN-2014) under grant agreement No. 642685 MacSeNet.

## VII. REFERENCES

[1] D. Lahat *et al.*, "Multimodal data fusion: An overview of methods, challenges, and prospects," *Proc. IEEE*, Sep. 2015.

[2] T. Adalı *et al.*, "Multimodal data fusion using source separation: Two effective models based on ICA and IVA and their properties," *Proc. IEEE*, Sep. 2015.

[3] S. Theodoridis, *Machine Learning: A Bayesian and Optimization Perspective*. Academic Press, 2015.

[4] Y. Levin-Schwartz, "Blind source separation for multimodal fusion of medical imaging data," PhD thesis, University of Maryland, USA, May 2017.

[5] M. A. Lindquist, "The statistical analysis of fMRI data," *Statistical Science*, Jun. 2008.

[6] S. Sanei and J. A. Chambers, *EEG Signal Processing*. John Wiley & Sons Ltd, 2007.

[7] E. Karahan *et al.*, "Tensor analysis and fusion of multimodal brain images," *Proc. IEEE*, Sep. 2015.

[8] D. Ramachandram and G. W. Taylor, "Deep multimodal learning," *IEEE Signal Process. Mag.*, Nov. 2017.

[9] S. Ferdowsi *et al.*, "A new informed tensor factorization approach to EEG–fMRI fusion," *J. Neuroscience Methods*, Oct. 2015.

[10] B. Hunyadi *et al.*, "Fusion of electroencephalography and functional magnetic resonance imaging to explore epileptic network activity," in *EUSIPCO-2016*.

[11] E. Acar *et al.*, "Tensor based fusion of EEG and fMRI to understand neurological change in schizophrenia," in *ISCAS-2017*.

[12] E. Acar *et al.*, "ACMTF for fusion of multi-modal neuroimaging data and identification of biomarkers," in *EUSIPCO-2017*.

[13] S. V. Eyndhoven *et al.*, "Flexible fusion of electroencephalography and functional magnetic resonance imaging: Revealing neural-hemodynamic coupling through structured matrix-tensor factorization," in *EUSIPCO-2017*.

[14] E. Martínez-Montes *et al.*, "Concurrent EEG/fMRI analysis by partial least squares," *NeuroImage*, Sep. 2004.

[15] V. Calhoun *et al.*, "Neuronal chronometry of target detection: Fusion of hemodynamic and event–related potential data," *NeuroImage*, Apr. 2006.

[16] W. Swinnen *et al.*, "Incorporating higher dimensionality in joint decomposition of EEG and fMRI," in *EUSIPCO-2014*.

[17] V. Calhoun *et al.*, "A review of group ICA for fMRI data and ICA for joint inference of imaging, genetic, and ERP data," *NeuroImage*, Mar. 2009.

[18] B. Mijović *et al.*, "The "why" and "how" of JointICA: Results from a visual detection task," *NeuroImage*, Apr. 2012.

[19] B. Hunyadi *et al.*, "Exploring the epileptic network with parallel ICA of interictal EEG and fMRI," in *EUSIPCO-2015*.

[20] F. Cong *et al.*, "Tensor decomposition of EEG signals: A brief review," *J. Neuroscience Methods*, Jun. 2015.

[21] A. H. Andersen and W. S. Rayens, "Structure-seeking multilinear methods for the analysis of fMRI data," *NeuroImage*, Jun. 2004.

[22] E. Acar *et al.*, "Multiway analysis of epilepsy tensors," *Bioinformatics*, Sep. 2007.

[23] C. Chatzichristos *et al.*, "PARAFAC2 and its Block Term Decomposition analog for blind fMRI source unmixing," in *EUSIPCO-2017*.

[24] L. Spyrou *et al.*, "Complex tensor factorization with PARAFAC2 for the estimation of brain connectivity from the EEG," arXiv preprint:1705.02019v1, May 2017.

[25] K. W. Andersen *et al.*, "Identifying modular relations in complex brain networks," in *MLSP-2012*.

[26] N. Sidiropoulos *et al.*, "Tensor decomposition for signal processing and machine learning," *IEEE Trans. Signal Process.*, Jul. 2017.

[27] D. Handweker *et al.*, "Variation of BOLD hemodynamic responses across subjects and brain regions and their effects on statistical analyses," *NeuroImage*, Apr. 2004.

[28] R. Bro and H. Kiers, "A new efficient method for determining the number of components in PARAFAC models," *J. Chemometrics*, May 2003.

[29] H. A. Kiers *et al.*, "PARAFAC2 — Part I: A direct fitting algorithm for the PARAFAC2 model," *J. Chemometrics*, May 1999.

[30] X. Lei *et al.*, "A parallel framework for simultaneous EEG/fMRI analysis: methodology and simulation," *NeuroImage*, Sep. 2007.

[31] N. Seichepine *et al.*, "Soft nonnegative matrix co-factorization," *IEEE Trans. Signal Process.*, Nov. 2014.

[32] M. Genicot *et al.*, "Coupled tensor decomposition: a step towards robust components," in *EUSIPCO-2016*.

[33] M. Sørensen *et al.*, "Coupled canonical polyadic decompositions and (coupled) decompositions in multilinear rank- $(L_{r,n},L_{r,n},1)$ terms — Parts I, II," *SIAM J. Matrix Anal. Appl.*, Jul. 2015.

[34] S. Sur and V. Sinha, "Event-related potential: An overview," *Ind. Psychiatric J.*, Jan. 2009.

[35] M. Weis *et al.*, "Temporally resolved multi-way component analysis of dynamic sources in event-related EEG data using PARAFAC2," in *EUSIPCO-2010*.

[36] L. Dong *et al.*, "Simultaneous EEG-fMRI: Trial level spatio-temporal fusion for hierarchically reliable information discovery," *NeuroImage*, May. 2014.

[37] E. B. Erhardt *et al.*, "SimTB, a simulation toolbox for fMRI data under a model of spatiotemporal separability," *NeuroImage*, Feb. 2012.

[38] L. Sorber *et al.*, "Structured Data Fusion," *IEEE J. Sel. Topics Signal Process.*, Jun. 2015.

[39] N. Vervliet *et al.*, "Tensorlab User Guide," 2016. [Online]. Available: http://www.tensorlab.net

[40] A. J. Bell and T. J. Sejnowski, "An information maximisation approach to blind separation and blind deconvolution," *Neural Comput.*, Nov. 1995.

[41] M. Morante *et al.*, "Information assisted dictionary learning for fMRI data analysis," arXiv preprint:1802.01334v1, Feb. 2018.

[42] "OpenfMRI." [Online]. Available: https://openfmri.org

[43] J. Walz *et al.*, "Simultaneous EEG-fMRI reveals temporal evolution of coupling between supramodal cortical attention networks and the brainstem," *J. Neuroscience*, Dec. 2013.

[44] K. R. Laurens *et al.*, "A supramodal limbic-paralimbic-neocortical network supports goal-directed stimulus processing," *Hum. Brain Map*, Jul. 2005.

[45] C. Chatzichristos *et al.*, "Higher-order block term decomposition for spatially folded fMRI data," in *LVA-ICA-2017*.